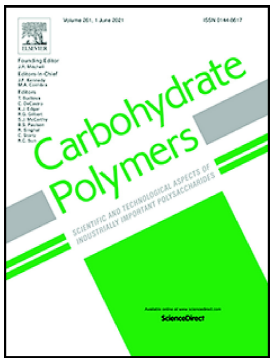

Hydration and dehydration induced changes in porosity of starch microspheres

Ramūnas Digaitis, Peter Falkman, Viveca Oltner, Lars-Erik Briggner, Vitaly Kocherbitov

PII: S0144-8617(22)00447-7

DOI: https://doi.org/10.1016/j.carbpol.2022.119542

Reference: CARP 119542

To appear in: *Carbohydrate Polymers*

Received date: 1 February 2022

Revised date: 12 April 2022

Accepted date: 24 April 2022

Please cite this article as: R. Digaitis, P. Falkman, V. Oltner, et al., Hydration and dehydration induced changes in porosity of starch microspheres, *Carbohydrate Polymers* (2021), https://doi.org/10.1016/j.carbpol.2022.119542

Hydration and dehydration induced changes in porosity of starch microspheres

Ramūnas Digaitis [1,2*], Peter Falkman [1,2], Viveca Oltner [3], Lars-Erik Briggner [3,4], and Vitaly Kocherbitov [1,2,**]

[1] Department of Biomedical Science, Malmö University, Malmö, Sweden

[2] Biofilms – Research Center for Biointerfaces, Malmö University, Malmö, Sweden

[3]Magle Chemoswed AB, Malmö, Sweden

[4]Adroit Science AB, Lund, Sweden

* Present address: Norwegian Institute of Bioeconomy Research, Ås, Norway

** Corresponding Author. Address: Department of Biomedical Science, Malmö University, SE-21432, Malmö, Sweden. E-mail: Vitaly.Kocherbitov@mau.se

Abstract

Characterization and tuning of the porosity of amorphous starch materials are important for many applications, including controlled release of encapsulated proteins. The porosities of these materials in dry and hydrated states can have different physicochemical origins and properties. Here, porosities of dry crosslinked starch microspheres and their hydration-induced transformations were characterized by small angle X-ray scattering, scanning electron and optical microscopies, thermogravimetric analysis, sorption calorimetry, nitrogen sorption, and helium-pycnometry. The analyses revealed that dry microspheres consist of porous cores with pore diameters below 100 nm and shells which appeared to be denser but contained wider pores (100-300 nm). The outer crust of the microspheres shell is non-porous, which restricts diffusion of nitrogen, water, and ethanol. Partial hydration triggered an irreversible collapse of dry porosity at 12 wt% water. Further hydration resulted in interfacial changes and promoted wet porosity, related to characteristic distances between polymer chains.

Keywords: Degradable starch microspheres; cross-linking; dry porosity; wet porosity; water sorption

1. Introduction

Controlled release of proteins typically relies on encapsulation or immobilization in a suitable delivery system. Delivery systems of preference are made up of natural, biocompatible, low-cost, and widely abundant polymers. Starch, fulfilling all delivery system requirements, is a polymeric carbohydrate consisting of two polysaccharides: the linear polymer amylose, composed of α-D-glucose units linked by α-D-(1–4) linkages, and the branched polymer amylopectin where α-D-glucose chains branch off at about every 24-30 glucose units by means of α-1,6 linkages (Whistler and Daniel 2000). The amylopectin chains fold into tight three-dimensional helical structures which collectively with amylose are further organized into granules where crystalline branching regions of amylopectin alternate with amorphous regions (Lourdin, Putaux et al. 2015, Cornejo-Ramírez, Martínez-Cruz et al. 2018). In the native state, starch granules are insoluble in cold water and the presence of crystalline regions limits drug delivery system applications (Sujka and Jamroz 2007, Builders and Arhewoh 2016). The crystalline structure can be disrupted by hydrothermal gelatinization that enhances the capacity of starch to interact with water (Ai and Jane 2015). Long polymeric chains of gelatinized starch can be fractionated to shorter chains by acid or enzymatic hydrolysis. Gelatinized starch can also be functionalized to prevent crystallization and to control swelling (Guo, Li et al. 2013, Uliniuc, Hamaide et al. 2013, Troncoso and Torres 2020). Chemical cross-linking resulting in the formation of inter-chain covalent bonds, may be used to maintain the disordered, amorphous structure of starch based materials (Wojtasz, Carlstedt et al. 2016). Cross-links prevent separation of individual polysaccharide chains, also upon hydration, and allow to produce particles of preferred dimension (Chung, Woo et al. 2004, Sandhu, Siroha et al. 2021). A large number of crosslinking agents for starch are known, including sodium trimetaphosphate (Fang, Wang et al. 2008), phosphoryl chloride (Kaur, Singh et al. 2006), and epichlorohydrin (Hamdi, Ponchel et al. 1998, Hirsch and Kokini 2002, Bendoraitiene, Lekniute-Kyzike et al. 2018). Due to their unique properties, cross-linked starch particles are attractive for pharmaceutical and biomedical applications, including drug delivery (Labelle, Ispas- Szabo et al. 2020). The drug loading capacity and the drug release rate may be tuned by controlling the physicochemical characteristics of cross-linked starch microspheres, *e.g.*, porosity, particle size, and degree of cross-linking, which taken together manage the diffusion of drugs and the swelling limits of the polymer matrix(Elfstrand, Eliasson et al. 2002, Kaur, Singh et al. 2006, Bendoraitiene, Lekniute-Kyzike et al. 2018, Sandhu, Siroha et al. 2021).

Various physical, chemical, and enzymatic modification methods have been applied to produce porous starch particles with porosity in the dry state (Zhu, Sun et al. 2018, Chen, Wang et al. 2020). Porosity can be classified according to the International Union of Pure and Applied Chemistry (IUPAC) system into *macropores* (width > 50 nm), *mesopores* (2 nm < width < 50 nm) and *micropores* (width < 2 nm) (Everett 1972). Micropores can be further subdivided into *ultramicropores* (width < 0.7 nm) and *supermicropores* (0.7 nm < width < 2 nm) (Everett 1972, Sujka 2017). Particle porosity increases surface area which is termed internal surface when pores and channels connect to the outer particle surface (Everett 1972).

During hydration of starch polymers water acts as a plasticizer, and above the glass transition, which at room temperature occurs when the water content of starch approaches 16-18% (Carlstedt, Wojtasz et al. 2014, Wojtasz, Carlstedt et al. 2016), starch microspheres swell and exhibit pronounced structural changes. These hydration-induced changes can affect porosity on multiple scales, and thus the permeability of the porous matrix (de Graaf, Karman et al. 2003). Hydration of porous starch microspheres induces transition from a dry state porosity, where pores of the dry material are filled with gases, to a wet-state porosity, where water occupies the volume between the polymer chains. The integrity of the swollen matrix is at the same time maintained by cross-linking. In the hydrated swollen state, the augmented wet porosity facilitates diffusion as well as partitioning of an active compound between the polymeric chains. The encapsulation of bioactive agents inside the starch microspheres can eventually be achieved by removal of water (Wulff 2021). During water removal, *e.g.*, by evaporation,

water present in spaces between microspheres is removed first, leading to the concentration of an active compound inside the particles. Upon further dehydration (drying), cross-linked starch microspheres recover to their initial dry shape. Rehydration of drug-loaded particles leads to swelling of the polymeric matrix triggering sustained diffusion of an active compound through the water swollen polymer matrix (Elfstrand, Eliasson et al. 2006, Fang, Wang et al. 2008). Starch is susceptible to hydrolysis by α-amylase, which is also present at a low level in blood (Labelle, Ispas- Szabo et al. 2020). Consequently, enzymatic disintegration may further be used to tune the release rate of an active compound from the particles (Hamdi, Ponchel et al. 1998, Bendoraitiene, Lekniute-Kyzike et al. 2018). Additional physical and chemical modifications may be introduced to fine-tune the release rate (Elfstrand, Eliasson et al. 2006).

There is a fundamental need to better understand the influence of porosity, cross-linking, hydration and dehydration induced transitions of starch particles to advance applications in the pharmaceutical industry. We hypothesize that dry and wet state porosities have different origins, different characteristic lengths, and that cross-linked starch particles undergo dramatic structural rearrangements under hydration, resulting in increased wet porosity which eventually governs drug encapsulation and release.

2. Materials and methods

2.1. Materials

Non-crosslinked maltodextrin (Glucidex 9) was kindly provided by Roquette (France). Degradable starch microspheres (DSM) of four different types were manufactured and provided in a dry state by Magle Chemoswed (Malmö, Sweden), Table 1. Starch microspheres were produced from acid hydrolyzed potato starch employing a water-in-oil emulsion technique and using epichlorohydrin as a crosslinking agent. Briefly: a solution of epichlorohydrin in toluene was added to an alkaline aqueous solution of hydrolyzed starch. Emulsification was performed at a specific concentration, temperature, duration, and stirring rate to obtain the desired starch droplet size. Once formed, the droplets were fixed by adding the crosslinking agent to the mixture. The same amount of the crosslinking agent per unit mass of starch was used for starch microspheres of types B, C and D. The formed microspheres were then purified through an extensive washing scheme, before being dried under vacuum at elevated temperature. Prior to further analysis, the microspheres were additionally dried at room temperature in vacuum with 3 Å molecular sieves for a 24 h period. DSM-A particles were partly described previously (Wojtasz, Carlstedt et al. 2016). The degradable starch microspheres of types B, C and D differ from DSM-A primarily in the degree of cross-linking. The cross-linking degree in DSM-A particles, unlike in DSM-B, DSM-C and DSM-D, was found to be insufficient to provide adequate robustness to enable the microspheres to maintain their integrity and recover their initial state after a hydration-drying cycle (Wojtasz, Carlstedt et al. 2016).

Table 1. Overview of degradable starch microsphere (DSM) properties

Name	Mean diameter in the swollen state (µm)	Amount of EtOH (%)	Density		Specific surface area		Volumetric swelling ratio (cm^3/cm^3)
			He-pycnometry (g/cm^3)	Geometrical (g/cm^3)	$S_{(BET)}$ (m^2/g)	$S_{(Geometrical)}$ (m^2/g)	
DSM-A	100	2	1.39	-	0.42	0.43	-
DSM-B	160	6	1.40	-	0.09	0.26	-
DSM-C	400	8	1.25	0.88	0.41	0.12	4.2 (0.8)
DSM-D	580	15	1.12	0.89	0.05	0.09	3.8 (0.5)

$S_{(Geometrical)}$ calculations are based on particle size and density values (He-pycnometry) reported in the table, assuming that DSMs are spherical. The amount of ethanol (EtOH) entrapped in the microspheres was determined using thermogravimetric analysis. Standard deviation, where applicable, is indicated in brackets.

In preliminary experiments, it was found that substantial amounts of residual ethanol were present in all microsphere batches, Table 1. Two different approaches were used to remove the residual ethanol from the microspheres. DSM particles were held in desiccators above saturated salt solutions for 24 h; first above NaCl, which provided a relative humidity (RH) of approximately 75.3%, and then above KNO_3, realizing a RH of 93.6%. This method was employed since significant mass loss was observed during measurements of sorption isotherms with a dynamic gravimetric moisture sorption analyzer. This approach removed substantial amounts of ethanol, but not all. Thus, another method, where an excess of liquid water was applied on dry microparticles, was used. After about 3 h of equilibration, the excess water was drained away and microspheres dispersed in Petri dishes (Ø 90 mm, made of glass) were dried at ambient room conditions for 3 days. The air-dried particles, and particles hydrated to certain RHs above saturated salt solutions, were dried in a desiccator in the presence of 3 Å molecular sieves for a 24 h period. Finally, the microspheres were dried under vacuum in the presence of dry molecular sieves, 3 Å, for a 24 h period at room temperature. Equilibration in liquid water enabled complete removal of ethanol from degradable starch microspheres (see results and discussion).

2.2. Methods

2.2.1. Scanning electron microscopy (SEM)

Surface morphologies as well as the internal structure of intact as well as mechanically crushed starch microspheres were studied using a Zeiss EVO LS10 (Oberkochen Germany) scanning electron microscope, operated at 25 °C in vacuum at an acceleration potential of 15 kV. Prior to measurements, the microspheres were deposited on graphite covered standard sample holders and sputter coated with a thin layer of gold.

2.2.2 Optical microscopy

Particle dimensions and swelling

A Nikon Optiphot optical microscope equipped with an Olympus UC90 digital camera (Tokyo, Japan) was used to determine the dimensions of dry and fully swollen microspheres and to investigate hydration-induced morphological changes. Dry microspheres were imaged by placing them on a microscopy glass slide. Swelling of microspheres was induced by applying a droplet of water. The diameter measurements of dry and fully swollen microparticles (DSM-C and DSM-D only, 6 and 10 individual microspheres, respectively) were carried out at three different angles and the average diameter values were used to calculate volumes of the microparticles. The volumetric swelling ratio of each microsphere was then determined by dividing the calculated volume of fully swollen microsphere by its volume prior to swelling. Densities of the DSM-C and DSM-D microspheres were determined by dividing the total mass of 6 or 10 dry microspheres by their total dry volume, Table 1. The hydration induced morphological changes were recorded on video, Video S1.

Heat induced transformations

A Linkam temperature control system LTS420 (Linkam Scientific Instruments, Tadworth, Surrey, UK) combined with the microscope was used to heat the microspheres up to 350 °C, 15 °C/ min, and to visualize heat induced transitions of the starch microspheres (Video S2).

2.2.3 Small-angle X-ray scattering (SAXS)

The microspheres were studied using small angle X-ray scattering with a Xenocs Xeuss 3.0 SAXS/WAXS system (Xenocs, Grenoble, France). The radiation was generated by a GeniX3D source (Cu Kα radiation). The beam collimation was performed using two sets of scatterless slits.

Measurements were performed in high resolution mode in vacuum. Scattering data were collected with a Pilatus 300K detector (Dectris, Switzerland). The scattering intensity I(q) is expressed as a function of the scattering vector q which is defined as $q = 4\pi \sin\theta / \lambda$ where 2θ is the scattering angle and λ= 1.54189 nm corresponds to the wavelength of the X-ray beam source. The measurements were carried out at two sample-to-detector distances, *i.e.*, 400 and 1700 mm, with an exposure time of 5 minutes at each distance. This resulted in a combined range of approximately $0.004 < q < 0.7$ Å^{-1}. Specimens were prepared directly in gel-holders by applying required amount of liquid water on dry starch microspheres or by absorbing water vapor from saturated salt solutions and sealing the gel-holders afterwards. A moisture leak test was performed by exposing the gel holders containing specimens to a vacuum for 5 min. Even though specimens which were found to leak during the test were not used, a minor mass loss after the SAXS measurement was observed in some cases. The moisture content of the specimens for the SAXS data reported here is given as an average value of moisture contents prior to and after the SAXS measurement.

Samples were studied at 25 °C. The scattering pattern from an empty gel-holder was used as the background in the data correction procedure. The data processing was done with the XSACT 2.4 software (Xenocs, Grenoble, France). The Gauss Lorentz Gel model (Yeh, Sokolov et al. 1998, Evmenenko, Theunissen et al. 2001) in the SasView 5.0.3 software was used to characterize hydrated starch microspheres.

2.2.4 Dynamic vapour sorption (DVS)

The dynamic moisture sorption of starch microspheres was investigated using a Q5000 SA sorption analyzer (TA Instruments-Waters LLC, New Castle, USA) at 25 °C. Initially, specimens were dried at 40 °C, 0% RH for 30 min using pre-heating in the instrument. Dry specimens were exposed to either 90 or 95% RH in incremental/ decremental RH steps of either 5 or 10%. Specimens were equilibrated at each RH level for either 60 or 120 min. One specimen (*ca* 3.5 - 6 mg) of each sample type was measured. Due to release of ethanol observed in the first runs, water sorption isotherms obtained in second consecutive runs were considered as characterizing the material purified from ethanol.

2.2.5 Nitrogen sorption

A Gemini 2375 (Micromeritics Instrument, Norcross, USA) instrument was used to determine the specific surface areas of crosslinked starch microspheres. The microspheres were placed into glass tubes and a continuous N_2 flow for 16 h was applied to remove molecules adsorbed on the external surface as well as from potential channels in the material. The actual saturation pressure for the liquid nitrogen used was determined simultaneously. After weighing the degassed samples, they were inserted into the measuring position at -196 °C (boiling point of liquid nitrogen), evacuated and then exposed to a range of partial pressures covering the range from 0.03 to 0.3 under adsorption mode. In order to ascribe the right amount of nitrogen to the substances, the free volume in the tubes was measured by He prior to nitrogen adsorption.

2.2.6 Helium Pycnometry

An AccuPyc 1330 (Micromeritics Instrument, Norcross, USA) instrument with He as the gas probe was used to determine the absolute density of crosslinked starch microspheres. The instrument was calibrated using a certified calibration kit where all necessary cell parameters were determined using a metal sphere of accurately known volume prior to the analysis. The specimens were tested directly after the specific surface area analyses and were thus considered as completely degassed. The specimen and container mass a (nominal volume of about 1 cm³, the container was filled up to 2/3) was carefully determined prior to the measurements. The absolute density ("true density" or "skeleton density") was determined using 10 purges (10 psig pressure), prior to the actual measurement, followed by 10 measurement runs for each specimen (10 psig pressure) and using the average as the result for the volume of the sample in the cup.

2.2.7 Thermogravimetric analysis (TGA)

Thermogravimetric analysis was carried out using a TGAQ500 (TA Instruments). A specimen (5−10 mg) placed in a platinum pan was suspended on a sensitive balance together with a reference pan. The specimen was then heated in a furnace with a heating rate of 10 °C/min (unless otherwise specified) under a N_2 atmosphere. The second weight loss step corresponding to the loss of ethanol was used to estimate the amount of entrapped ethanol in the microspheres.

2.2.8 Sorption calorimetry

Hydration of starch microparticles was also investigated with sorption calorimetry which simultaneously measures water activity and hydration enthalpy at a constant temperature (Wadsö and Markova 2002). The measurements were made in a two-chamber calorimetric cell at 25 °C. To prevent specimen hydration prior to the measurement, vacuum dried starch microspheres were loaded into the sorption chamber inside a glovebox where a dry atmosphere (<5% RH) was maintained with nitrogen gas. The experiment was initiated by injecting water in the vaporization chamber from which vapor diffused to the sample placed in the sorption chamber. The thermal powers from the two chambers are recorded simultaneously and were used to calculate the water activity and the partial molar enthalpy of mixing of water (Kocherbitov 2021).

2.2.9 Differential scanning calorimetry (DSC)

Differential scanning calorimetry (DSC 1, Mettler Toledo, Schwerzenbach, Switzerland) was used to determine the amount of non-freezing water in starch microspheres. Specimens equilibrated to different hydration levels were hermetically sealed in aluminum pans (40 µL, Mettler Toledo). The sealed specimens were cooled from room temperature to -70 °C, held at this temperature for 5 min, and subsequently heated to temperatures ranging from 90 to 130 °C at a scanning rate of 10 °C/min. Indium was used as a calibrant, and an empty sealed aluminum pan was used as a reference. The non-freezing water contents were calculated from the linear dependence of the enthalpy of melting of ice (ΔH) on the concentration of water, after extrapolation of ΔH to 0 (Wojtasz, Carlstedt et al. 2016).

2.2.10. Particle size measurements

A Mastersizer 2000 (Malvern Panalytical, UK) was used to determine swollen state particle sizes by suspending DSM in 0.9% NaCl solution.

3. Results and discussion

3.1. Morphology and porosity of dry crosslinked starch microspheres

Characterization of structural features of crosslinked starch microspheres is important for understanding their behavior during encapsulation of active compounds. SEM images revealed that the starch microspheres had different sizes and morphologies, Figure 1. The DSM-A particles had wrinkled surfaces, whereas surfaces of DSM-B, DSM-C, and DSM-D particles were relatively smooth but contained irregularly distributed patches where pore-like structures could be seen, Figure 1. The batch C microspheres were found to have more shape irregularities than the microspheres from the batches B and D. A lower cross-linking degree of the DSM-A particles is likely the major factor responsible for the wrinkled surface topology of dry particles (Liu, Liu et al. 2019). A broad size distribution of the crosslinked starch microspheres in each batch was observed where smaller particles often aggregated with larger particles, Figure 1.

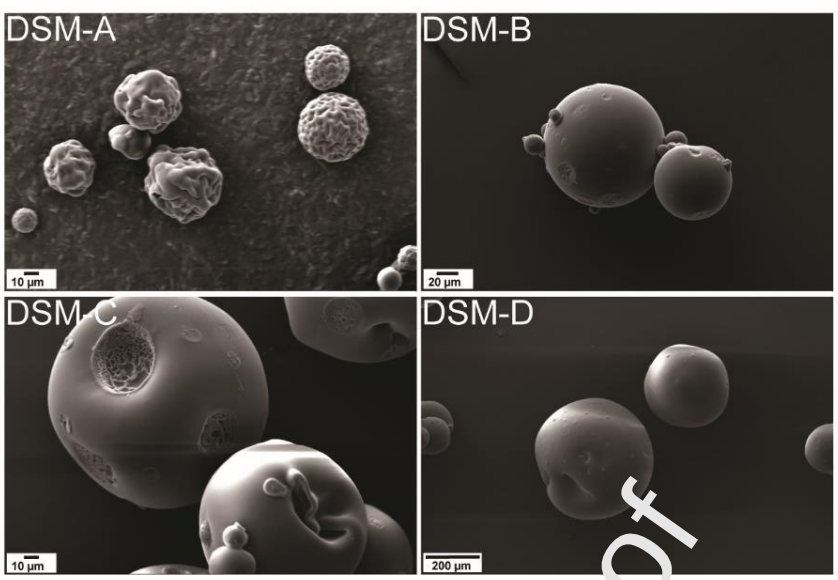

Figure 1. SEM images of degradable starch microspheres (DSM) prior to ethanol removal.

SEM imaging of crushed particles revealed that the defects were limited to the surface only, i.e. the pore-like ducts did not proceed into the particles, Figure 2 a, b. Nevertheless, the images revealed that the microspheres were porous, and three layers: a core, a shell, and a crust can be identified, Figure 2, c, d, and Figure S1, a, b. The pores in the cores appear to be <100 nm in diameter while shells seemed to be denser but contained wider pores (100-300 nm). No macropores were present in the about 1.5 µm thick outer crust of the microspheres. It was also found that pores in the shells of microspheres from batch C were more abundant than in the shells of the microspheres from the batches B and D. Large voids, in the range of 1-2 µm, were also present but these were less abundant and typically located in the cores of the microspheres, Figure 2, a, c and Figure S1, c, d. From the SEM images it is not evident if the pores were voids or connecting channels and if the outer crust of the microspheres contained micropores.

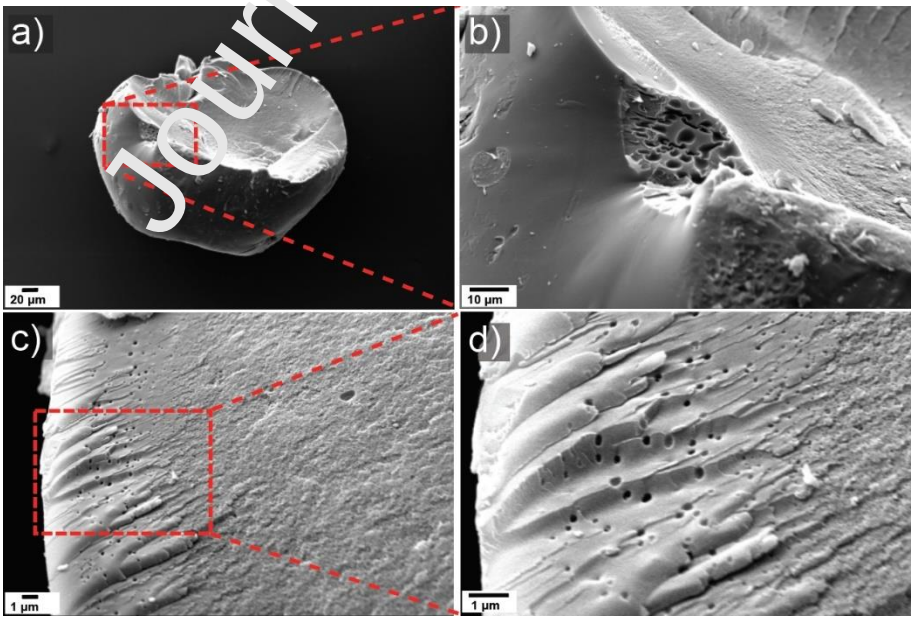

Figure 2. SEM images of mechanically crushed starch microspheres (prior to ethanol removal). Images a) and b) indicate that pore-like ducts visible on the surfaces of the microspheres did not proceed into

the particles (DSM-D). Images c) and d) indicate that microspheres consist of friable cores, denser shells containing fewer but larger voids and a non-porous outer crust (DSM-C).

The specific surface areas determined with BET, ($S_{(BET)}$), revealed that microspheres from all batches had small specific surface areas, similar to the theoretically calculated values ($S_{(Geometrical)}$), which were calculated based on the assumption that the particles were spherical (Table 1). The data confirmed that microspheres had a tight crust, restricting nitrogen molecules to access pores beneath the crust. Compared with $S_{(Geometrical)}$, the somewhat higher $S_{(BET)}$ values recorded for DSM-C may be due to the distorted and less smooth surface of the particles (Figure 1), but also minor contribution from the internal cavity surface cannot be ruled out. Also, since the mean particle size of each batch was used to calculate $S_{(Geometrical)}$ values, the minor discrepancies between measured and calculated specific surface areas may be due to the wide particle size distribution in each batch.

The density values determined with He-pycnometry ranged between 1.12 – 1.4 g/ cm^3 (Table 1) and thus were lower than the literature value of density of starch without hidden pores, *i.e.*, 1.5 g/cm^3 (Isleib 1958). During the measurement it was noted that the progress of the measurement was relatively slow, suggesting that helium atoms, which are smaller than nitrogen molecules, were able to diffuse beyond the outer crust of the microspheres providing densities that were close to the value of starch; therefore, another method, based on mass and particle dimension measurements with light microscopy, was also used to calculate the density of DSM-C and DSM-D particles. The density values calculated based on mass and size (determined with optical microscopy) were found to be substantially lower, 0.88 and 0.89 g/cm^3, respectively. Even though in optical microscopy the particle size can be overestimated because the image of a dry particle is its projection, the obtained density values indicate a porous structure of dry starch microspheres.

3.2. Mechanisms of temperature-induced weight loss

During thermogravimetric analysis it was found that small amounts of a trapped compound, which was identified as ethanol, were present in all microsphere batches. During synthesis of starch microspheres ethanol is used to displace water (Chen, Wang et al. 2020), that upon evaporation or removal by freeze drying is known to induce pore formation (Gao, Li et al. 2013, Oliyaei, Moosavi-Nasab et al. 2019). Thermograms in Figure 3a revealed up to three weight loss steps where the first step started at about 40 °C and was due to the loss of water. The second weight loss step corresponded to the loss of ethanol and was used to estimate the amount of entrapped ethanol, which was found to correlate with the size of the particles, *i.e.*, the largest microspheres (DSM-D) contained the largest amount of ethanol (ca. 15 wt%), Table 1. The temperature at which release of ethanol commenced was also affected by the amount of entrapped ethanol. Ethanol release from the particles containing larger amounts of ethanol commenced at lower temperatures and for the microspheres containing the largest amounts of ethanol (DSM-D and DSM-C), evaporation of water and ethanol overlapped, Figure 3a. The third weight loss step occurred at about 300 °C and was due to the pyrolysis of starch (Kaczmarska, Żymankowska-Kumon et al. 2019), Figure 3a.

The reason why ethanol remained trapped in dry microspheres is likely a combination of its slow diffusion, lack of porosity in the crust, and affinity to starch polymers. Possibly, the polymer chains were arranged so tightly in dry microspheres, in particular within the microsphere crust, that the free volume needed for larger ethanol molecules to move was limited, even though ethanol molecules form fewer hydrogen bonds with starch than water (a water molecule can donate two hydrogen bonds while ethanol only one). The diffusion of ethanol out of the microspheres was possibly also limited by ethanol embedment in amylopectin helixes leading to a potential hydrophobic interaction between glucose units and ethanol (Immel and Lichtenthaler 2000). The presence of ethanol in the microspheres may also explain why the density values (determined with He-pycnometry) of porous starch microspheres were relatively high. Ethanol, despite having lower density, may increase the density of starch by filling small voids between the polymer chains.

During the TGA analysis of the largest microspheres (DSM-D), an abrupt mass loss at approximately 165 °C was observed. Light microscopy studies revealed that the largest particles, which contained the highest amount of ethanol, burst at approximately 165 °C, and flew away from the original position (Video S2), which explains the sudden mass loss seen in the thermogram recorded with a heating rate of 10 °C/min (Figure 3a). The microscopy observations revealed swelling of the microspheres followed by rapid formation of bubbles inside the particles, just prior to disintegration (Video S2). This observation confirmed that shells of the microspheres had denser and less permeable structure and that channels extending from the core towards the microsphere surface were absent. The disintegrations likely occurred when shells of the microspheres no longer could withstand the pressure of the ethanol vapor. The bursts were significantly less pronounced for smaller particles containing less ethanol and when the heating rate was reduced to 1 °C/min, suggesting that the vapors were gradually diffusing through the denser crust of the microspheres, Figure 2 c). The morphological transformations of crosslinked starch microspheres occurring at the same temperature range as the ethanol loss observed with TGA indicate that both phenomena can be induced by the glass transition of starch.

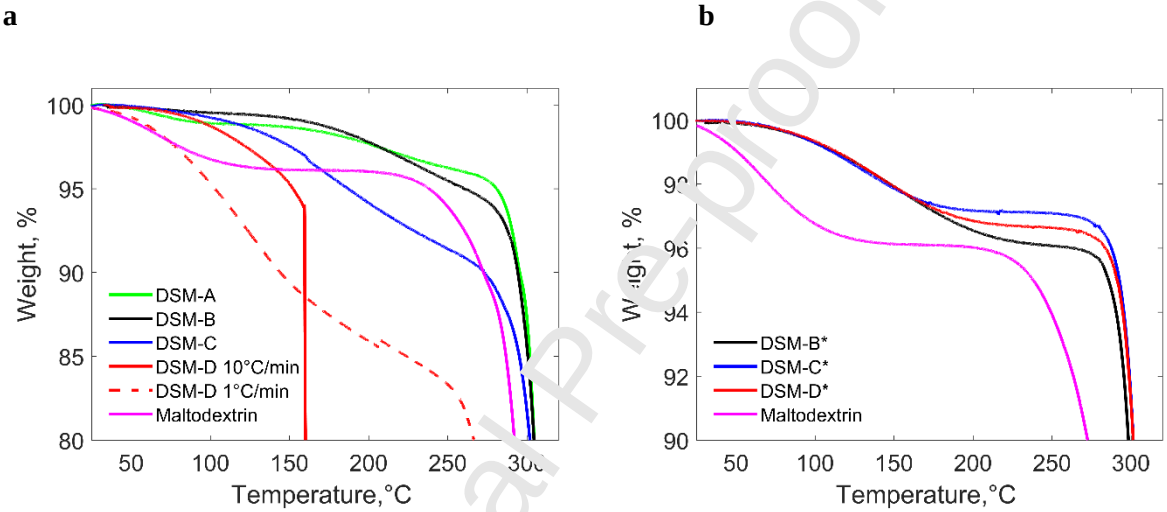

Figure 3. TGA results of starch microspheres a) containing ethanol and b) without ethanol, *i.e.*, the ethanol was removed by liquid water. All specimens were subjected to a heating rate of 10 °C/min. The DSM-D particles were also analyzed with a heating rate of 1 °C/min. A thermogram of a reference starch sample, maltodextrin, which neither contains ethanol nor cross-links is included for comparison. * indicates ethanol free particles.

After removal of ethanol from the microspheres (see section below) the TGA profiles provided additional information which was initially partly shielded by the ethanol loss step. Specifically, the size of the microspheres had no effect on pyrolysis temperature. Furthermore, pyrolysis of starch microspheres crosslinked to different degrees (cross-linking degree in DSM-A was lower) occurred at the same temperature. Nevertheless, the comparison of TGA profiles of crosslinked starch (microspheres) with a non-crosslinked starch reference, maltodextrin, indicated that cross-linking increases the temperature at which pyrolysis of starch occurs, *i.e.*, cross-linking raised the onset temperature of pyrolysis by approximately 60 °C, Figure 3 b). In agreement with this data, crosslinking by various crosslinking agents has been previously found to increase the thermal stability of starch (Reddy and Yang 2010, Singh and Nath 2012, Gao, Li et al. 2014).

3.3. Mechanisms of water-induced transformations – loss of dry porosity

3.3.1. Optical microscopy observations

Optical microscopy studies revealed that when exposed to liquid water the crosslinked starch microspheres started to swell and an advancing water front towards the center of the particle was visible during the swelling (Figure 4, Video S1), indicating case II diffusion (Li and Lee 2006). It could be

noted that dry particles containing ethanol and particles from which ethanol was removed scattered light differently. Specifically, ethanol containing particles appeared significantly less transparent, likely due to light scattering by the pores. Once fully hydrated, however, both types of particles were transparent and appeared identical, Figure 4. Optical microscopy studies also revealed the presence of pores in ethanol-containing (original) microspheres, that during the swelling process were visible in a form of variously sized bubbles, indicating entrapped gases. The gas bubbles likely emerged from the pores which were observed in dry particles (Figure 2), and during hydration of the cross-linked starch matrix, the gas bubbles coalesced before gas diffused out from the microspheres. Extended swelling of the crosslinked starch matrix mostly allowed gradual diffusion rather than a sudden release of the entrapped gasses, indicating that a fairly rigid structure of starch microspheres was realized by cross-linking. The extent of the DSM-C and DSM-D particle swelling was found to be similar; the determined volumetric swelling ratios were 4.2±0.8 and 3.8±0.5, respectively (Table 1), but lower than the degree of swelling of DSM-A particles (Wojtasz, Carlstedt et al. 2016), reflecting the fact that DSM-A is less cross-linked.

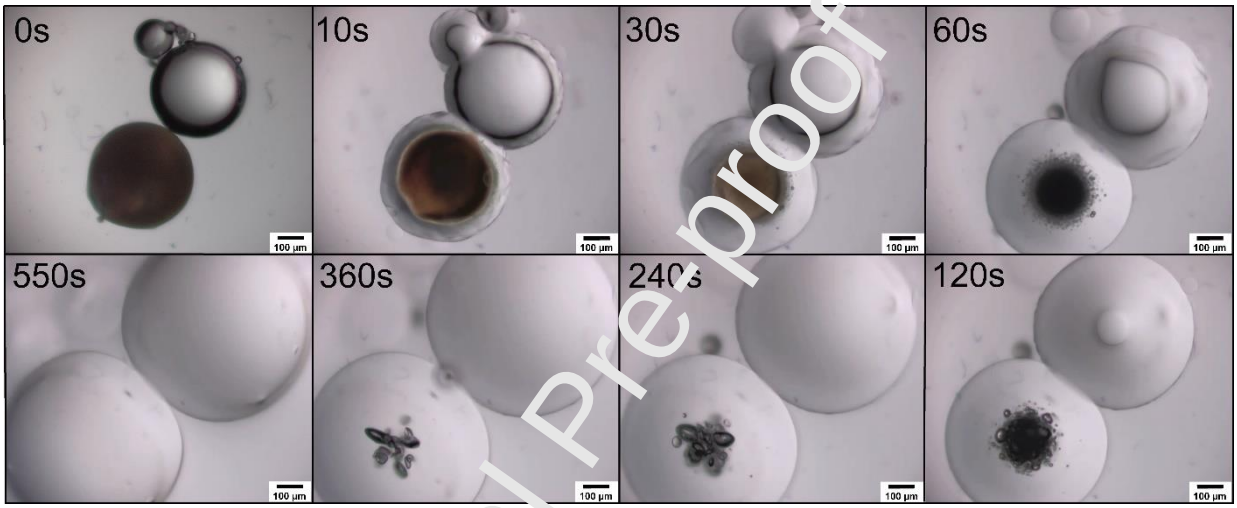

Figure 4. Swelling of DSM-D particles. Ethanol containing microspheres appear darker than microspheres of the same batch from which ethanol was removed by liquid water. Prior to imaging, both particles were vacuum dried for 24h in the presence of 3 Å molecular sieves. Swelling was initiated by applying a droplet of ultra-pure water on top of the particles.

Notably, entrapped gas bubbles were no longer visible during swelling of microspheres from which ethanol was removed by liquid water, Figure 4. Correspondingly, SEM images confirmed that the internal porosity seen in the original materials was absent in the microspheres from which ethanol was removed, Figure 5. The ethanol removal procedure did not significantly affect the overall shape of microspheres from the batches C and D. The areas where hydrated microspheres touched each other, or a glass surface of a Petri dish, during drying were visible, but unlike for the original microspheres no pore-like structures within these areas could be seen, Figure 5. On the contrary, morphology of the smaller microspheres (DSM-B) having similar degree of cross-linking as the larger particles (DSM-C and DSM-D) was affected significantly. The DSM-B microspheres formed large aggregates, Figure 5. In the dry state the microspheres within the aggregates could not be easily separated. When force was applied the aggregates tended to break as a single unit, Figure S4. During drying, the smallest particles, DSM-A, which also had the lowest degree of cross-linking, aggregated in such a way that their spherical structure was lost (data not shown).

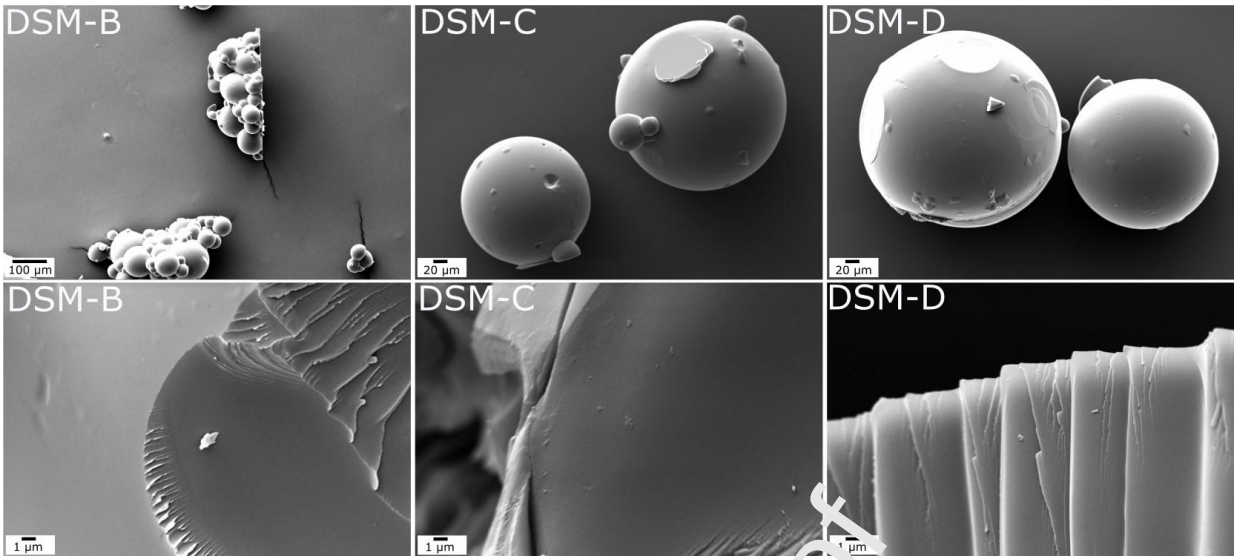

Figure 5. SEM images of starch microspheres from which ethanol was removed with liquid water. Intact and crushed microspheres in upper and lower rows, respectively.

3.3.2. Hydration of starch microspheres studied by sorption calorimetry, DVS and DSC

During DVS water sorption experiments, the presence of ethanol in the microspheres was observed as a pronounced mass loss when the RH was ramped above 50%. After the water absorption-desorption cycle, the mass of the material was substantially lower than the initial sample mass indicating that ethanol evaporated from the microspheres at high humidity, Figure S2 a). During the second consecutive measurement no moisture induced mass loss was observed, indicating that water displaced ethanol, triggering effusion from the particles by hydration and swelling of the polymer matrix. Sorption isotherms, based on the data from the second consecutive measurement, revealed that DSM-B, DSM-C, and DSM-D microspheres had comparable moisture sorption characteristics, Figure S3. A small sorption-desorption hysteresis was seen in DVS experiments with particles of all three types, see supporting info for details. Even though exposure to water vapor resulted in substantial removal of ethanol, treatment of the particles with liquid water was more efficient and hence used when required to purify the material from traces of ethanol.

The sorption calorimetry data for original (containing ethanol) microspheres and microspheres from which ethanol was removed by liquid water are shown in Figure 6 (a, c and b, d respectively). The enthalpy plots indicate that initial hydration of starch microspheres is an exothermic process. Noteworthy, another exothermic event was visible when water content of the ethanol containing microspheres reached 7-10%, Figure 6.c). The exothermic peak, however, was not present in the hydration enthalpy curves of the corresponding microspheres without ethanol, Figure 6.d). The peak, therefore, represents ethanol substitution by water. The magnitude of the exothermic peak was found to correlate with the amount of ethanol entrapped in the differently sized microspheres (Table 1), where the area of the exothermic peak was smallest for the smallest particles and largest for the largest particles, Figure 6.c). Wojtasz *et al*. previously reported hydration enthalpy data for the DSM-A particles, most likely due to a comparatively small amount of ethanol in these microspheres, the ethanol induced exothermic peak is however not pronounced in the enthalpy plot of DSM-A (Wojtasz, Carlstedt et al. 2016), (Table 1). The position of the exothermic peak is shifted towards lower water content for the DSM-C microspheres, Figure 6.c).

Sorption isotherms in Figure 6.a show that DSM-C absorbed water faster than DSM-B and DSM-D during the initial sorption period. SEM images of crushed particles indicated that voids in the shells of the DSM-C particles were most abundant, Figure 2, which potentially triggered faster diffusion of water vapour into the microspheres, concurrently inducing counter diffusion of ethanol at lower moisture

contents. A step in the enthalpy curves at approximately 18% of water content can be clearly seen for particles from which ethanol was removed, Figure 6. d. The corresponding step of original, ethanol containing microspheres, occurring at approximately 17% water content, overlaps with the exothermic peak in the enthalpy curves. This step signifies the glass transition of starch (Carlstedt, Wojtasz *et al*. 2014, Wojtasz, Carlstedt *et al*. 2016). It is well established that the glass transition temperature of starch-based materials is strongly dependent on water content and reaches room temperature when the moisture content of starch approaches 18% (Wojtasz, Carlstedt *et al*. 2016). The water content at which the glass transition occurred in original microspheres is slightly lower, indicating that ethanol, like water, acted as a plasticizer. Interestingly, ethanol evaporation was induced before the glass transition of the polymer. The data thus suggest that the swelling, although mechanically demanding, occurred in the glassy state to an extent sufficient for the mobility of ethanol molecules. Data in Figure 6.b) indicate that the size of starch microspheres also influenced water sorption. Hence, since the ethanol removal procedure induced aggregation of DSM-B particles (Figure 5), the particles which initially were smaller than DSM-C and DSM-D (Table 1) became the largest ones (Figure 5). With increasing water activity, the water content of these aggregates increased at the lowest rate. Similarly, larger DSM-D microspheres absorbed water at a lower rate than smaller DSM-C particles. After mechanical grinding, which caused breakup of particle aggregates as well as fragmentation of individual particles, the DSM-B specimen absorbed water at the highest rate, Figure 6 b.

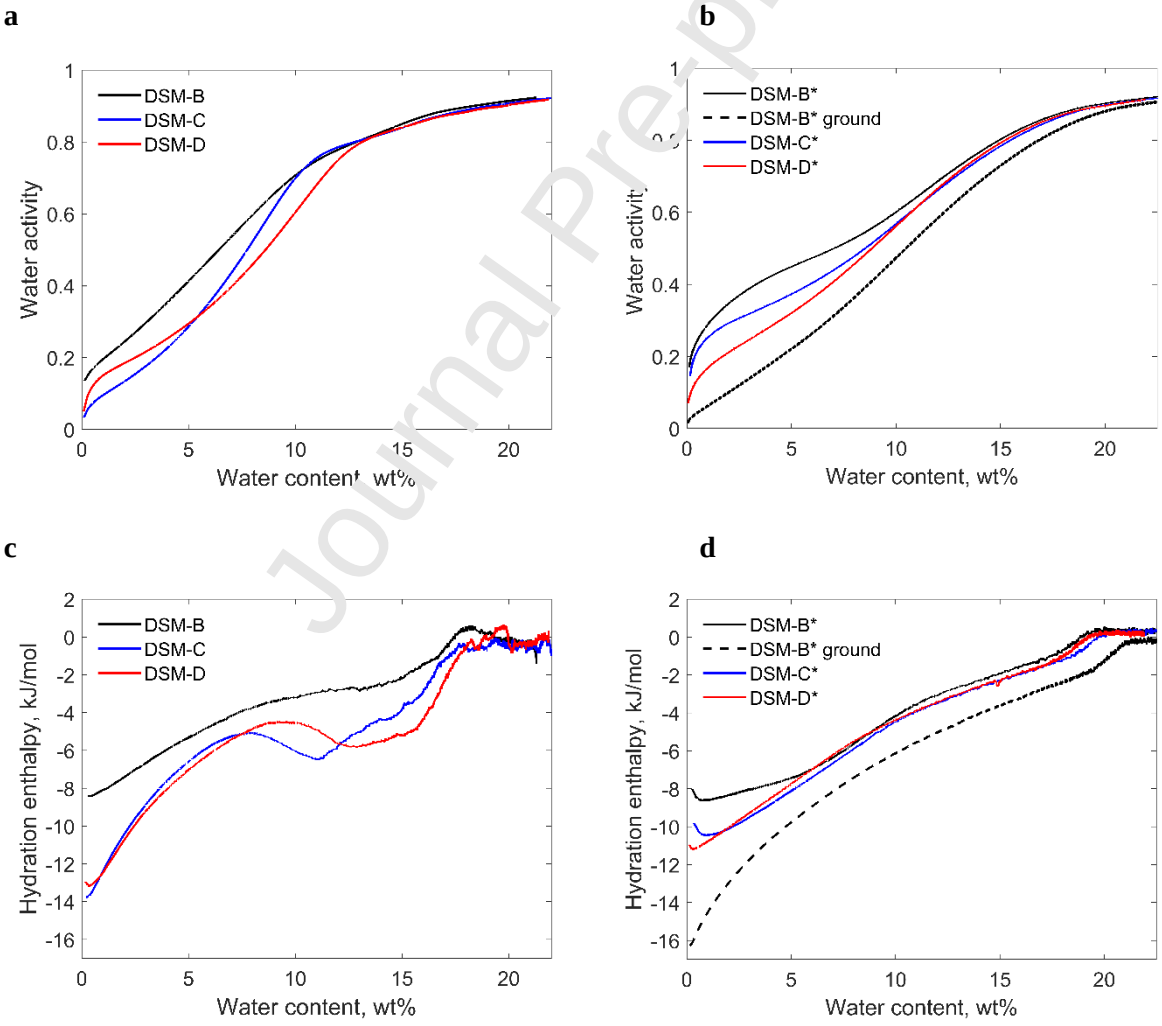

Figure 6. Water sorption isotherms (a) and enthalpies of hydration (c) of untreated starch microspheres containing ethanol. Subplots c and d show corresponding data for starch microspheres from which

ethanol was removed by liquid water. Dashed curves represent data from ground particles. * indicates ethanol free particles.

The amount of non-freezing water in DSM-B particles, determined by DSC, was found to be 29.1 wt.% (Figure S5). A similar amount of non-freezing water, 27.4 wt%, has been previously reported for DSM-A particles (Wojtasz, Carlstedt et al. 2016).

3.3.3. From dry to wet porosity, SAXS observations

Figures 7, S5, and S6, show small-angle X-ray scattering data obtained from starch microspheres hydrated to different extents.

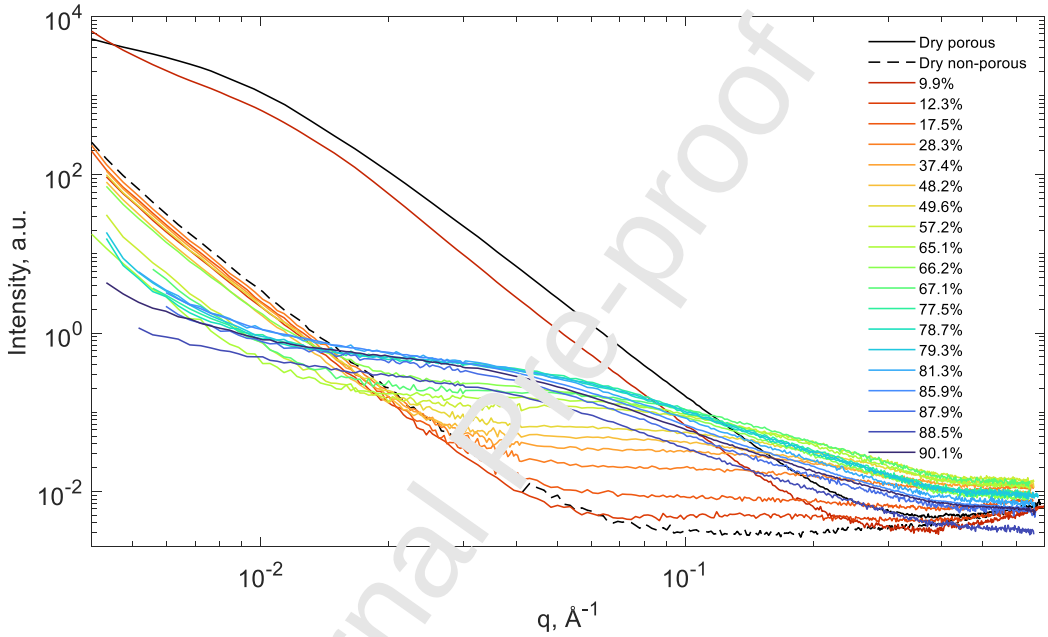

Figure 7. Small-angle X-ray scattering data of dry DSM-C particles containing ethanol, and particles hydrated to different moisture contents. The dashed curve indicates scattering from dry DSM-C particles treated with liquid water.

SAXS provides structural information at different length scales and the total X-ray scattering intensity I is the sum of the scattering contributions from external and internal particle surfaces (pores): $I_{surf(ext)}$ and $I_{surf(pores)}$, respectively, starch chains (I_{chains}), and individual glucose units of starch chains ($I_{glucose}$):

$$I = I_{surf(ext)} + I_{surf(pores)} + I_{chains} + I_{glucose} \quad (1)$$

No Bragg peaks could be detected in the whole water content range tested, indicating that cross-linking prevented crystallization of glucose chains, a known occurrence in non-crosslinked starch (Carlstedt, Wojtasz et al. 2014). Notably, the scattering pattern and intensity was affected substantially by water content, which lead to both sudden and gradual changes in the X-ray scattering pattern. The SAXS data (Figures 7, S6 -S7) together with optical microscopy observations (Figure S8) suggest four different states and three transitions, summarized in Table 2.

Table 2. Moisture-induced transformations of cross-linked starch microspheres based on SAXS and light microscopy observations

H_2O conc. range (%)	State of microspheres	Dominating Interface	Transition Event	Scattering intensity change in transition	
				Low q ($0.0005\ A^{-1}$)	Higher q ($0.07\ A^{-1}$)
0-12	Solid, glassy, porous, non-transparent, in air	Solid surface in pores - air	-		
12-56	Non-porous, soft, undergoing swelling, increasingly transparent, in air	Soft particle - air	Collapse of dry pores/ pore filling	↓	↑
56-90	Soft, deformed in constrained environment, increasingly transparent	Soft particle - particle	Formation of flat interfaces between adjacent particles	↓	↑
>90	Fully swollen, transparent, spherical in liquid environment	Soft particle water	Microspheres regain spherical shape	↓	↓

Symbols ↑ and ↓ indicate increase and decrease of X-ray scattering intensity, respectively.

Porous microspheres, dry or hydrated up to approximately 12 wt% water scattered X-rays at high intensity at lower *q* values and scattering from the air-solid interface in pores was dominant. In SAXS, the air-solid surface interface provides a good contrast and thus high intensities at low q values. The slope of the broad linear region was close to -4, corresponding to a surface fractal dimension of 2, which indicates a smooth surface (Wojtasz, Carlstedt et al. 2016).

First transition occurred at water content of 11.8 wt% (approximately 12 wt%), which is seen as a strong, two orders of magnitude loss of scattering intensity, Figure 7. This dramatic loss of scattering intensity seems to occur slightly before the glass transition of the material, close to the exothermal peak interpreted as evaporation of ethanol (Figure 6 c). The significant loss of scattering intensity from the gas-particle interface, can be associated with two events: (i) collapse of pores due to the softening of the polymer matrix and (ii) pore filling, *i.e.*, condensation of water vapor in the pores. Undoubtedly, the moisture induced mobility of the polymeric material, driven by minimization of free energy, leads to a collapse of the dry state pores (Figure 5), resulting in a decrease of the gas-starch interface, but whether collapse of the pores occurred prior to the glass transition, is unclear. Condensation of water vapor in the pores, on the other hand, may occur since polymer swelling in the glassy state is constrained. The point at which condensation of water vapor in macroscopic voids occurs can typically be elucidated from sorption isotherms since condensation leads to a sudden increase in water content of a porous material (Fredriksson and Thybring 2019). Regarding the porous starch microspheres, which also

contained ethanol, gravimetrically obtained moisture sorption data is however of little value due to the evaporation of ethanol, Figure S2. In sorption calorimetry, water uptake by the material is determined from the heat production rate during vaporization of water in the vaporization chamber and absorption of the same vapor by the material in the sorption chamber (Nopens, Wadsö et al. 2019, Kocherbitov 2021). Nevertheless, the presence of ethanol in the sample also influences sorption isotherms determined with sorption calorimetry since ethanol vaporization from the sample as well as its diffusion to the (water) vaporization chamber induce thermal events which cannot be distinguished from thermal events caused by vaporization and sorption of water. Still, a levelling of the sorption isotherm, consistent with capillary condensation/ filling of pores could be observed at 11.4 wt.%, Figure 6.a.
The interpretation of the scattering intensity loss as related to either the collapse of pores or pore filling with water (and/or ethanol, which becomes mobile at ca. 7-10 wt% moisture (Figure 6 A)) is supported by the fact that the X-ray scattering intensity from microspheres which lack porosity was in the same range as the intensity from original microspheres hydrated above 11.8 wt% moisture, Figures 7, S5. Original starch microspheres hydrated to ca. 10 wt% moisture, on the other hand, scattered X-rays at lower intensity, but still comparable to the dry porous microspheres, Figures 7, S6-7. From the SEM images it is evident that a wide size distribution of pores was present in original dry microspheres, Figure 2. The slope of the SAXS intensity arising from dry porous microspheres deviates from the value of -4 at q values $<10^{-2}$ Å^{-1}, which may indicate that the corresponding distance of 60 nm indicates the approximate dry pore size. Fitting of the data using a cylinder model did not, however exhibit a good fit (data not shown), probably due to a variety of pore shapes.

After the first transition, the scattering intensity and the slope at lower q values remained fairly stable until approximately 56 wt% of water. A gradual increase in scattering intensity at higher q values was, on the other hand observed in the 12-56 wt% moisture range, Figures 7, S6-7. The scattering at higher q values arises from the polymer chains. The Gauss Lorentz Gel model (equation 2), which is found to be appropriate to describe scattering from chemically crosslinked gels (Yeh, Sokolov et al. 1998, Evmenenko, Theunissen et al. 2001), was used to characterize starch microspheres hydrated to different moisture contents.

$$I(q) = I_G(0)\exp\left(-\frac{q^2\Xi^2}{2}\right) + \frac{I_L(0)}{1+q^2\xi^2} \qquad (2)$$

Ξ is the length scale of the static correlations in the gel, which can be attributed to the crosslinks. ξ is the dynamic correlation length, which can be attributed to the distances between fluctuating polymer chains, *i.e.*, mesh size or wet porosity. $I_G(0)$ and $I_L(0)$ are the scaling factors for each of these structures. By fitting the experimental data to this equation static and dynamic correlation lengths were obtained, Figure 8, Table S1. The fitting curves agreed with the experimental data for all DSM-B, DSM-C and DSM-D particles equilibrated to different moisture contents. The static correlation lengths values were found to be much greater than the dynamic correlation lengths, in agreement with the parameters reported for cross-linked polymer gels in other studies (Yeh, Sokolov et al. 1998, Evmenenko, Theunissen et al. 2001). The data indicate that at low hydration levels (. <40 wt% water) the cross-linked starch chains are tightly arranged, *i.e.*, the characteristic mean distance between the chains being less than 5Å, Figure 8 b. With increasing degree of hydration, the dynamic correlation length values increased gradually, reaching about. 48 Å (Figure 8 b), representing sufficient porosity to encapsulate smaller proteins and allow their diffusion. The dynamic correlation length values agreed well for all three microsphere batches, which means that distances between starch chains at different hydration levels were similar in all particles.

a **b**

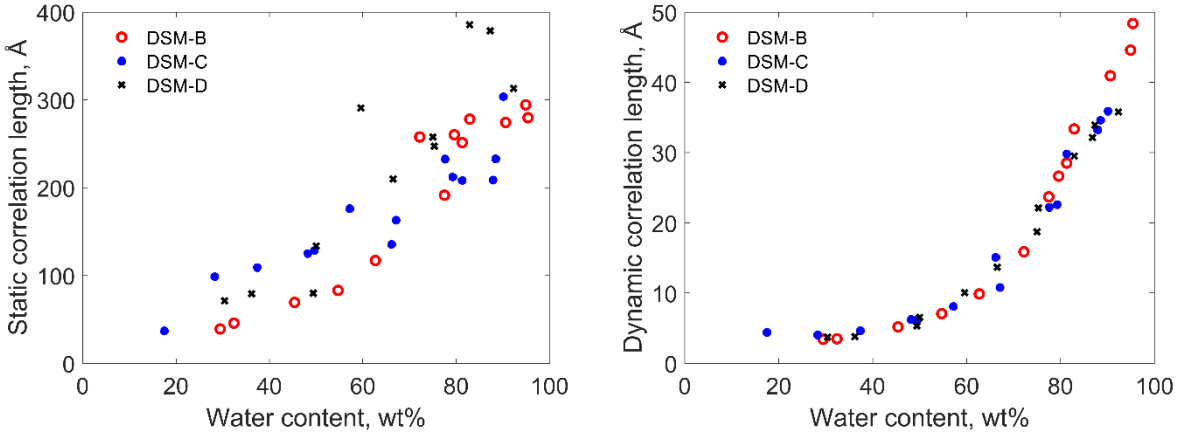

Figure 8. Static and dynamic correlation lengths of DSM particles equilibrated to different water contents. Correlation values were obtained by fitting the SAXS experimental data with the Gauss Lorentz Gel model.

The second pronounced transition, *i.e.*, loss of scattering intensity in the low *q* range, occurred at approximately 56 wt% moisture, Figures 7, S6-7. When that moisture content was reached, adjacent microspheres in the constrained environment mutually adjusted their shapes by forming flat interfaces (Figure S8), as typically seen in foams (Drenckhan and Saint-Jalmes 2015). At increasingly higher water contents, water started to fill spaces between adjacent microspheres that were previously occupied by gas, and above about 90 wt% water, particles recovered a spherical shape (Figure S8), which in SAXS was seen as an overall decrease in scattering intensity, Figures 7, S6-7.

Conclusions

Porosity of cross-linked starch particles is essential for encapsulation and controlled release of active compounds. The present study has revealed that porosities of dry and hydrated cross-linked starch particles have different origins and characteristic lengths. Dry microspheres were found to consist of porous cores with pore diameters below 100 nm, shells that appeared to be denser, but with wider pores (about 100-300 nm), and a non-porous outer crust, which restricted diffusion of nitrogen, water, and ethanol. Partial hydration triggered a dry porosity collapse at about 12 wt% water. Up to approximately 40 wt% water, the crosslinked starch chains were compactly arranged, with distances between the chains being below about 3 Å. Further increase in hydration promoted gradual increase in characteristic distances between polymer chains, *i.e.*, wet porosity, where the dynamic correlation length between chains reached 48 Å at about 95 wt% water, sufficient for immobilization and diffusion of variety of higher molecular weight compounds such as proteins.

Acknowledgements

This work was financially supported by the Knowledge foundation (KK-stiftelsen). Authors acknowledge fruitful discussions with Peter Schuisky. Juan Francisco Gonzalez-Martinez is acknowledged for assistance with SAXS measurements.

References

Ai, Y. and J. l. Jane (2015). "Gelatinization and rheological properties of starch." Starch-Stärke **67**(3-4): 213-224.

Bendoraitiene, J., E. Lekniute-Kyzike and R. Rutkaite (2018). "Biodegradation of cross-linked and cationic starches." International journal of biological macromolecules **119**: 345-351.

Builders, P. F. and M. I. Arhewoh (2016). "Pharmaceutical applications of native starch in conventional drug delivery." Starch-Stärke **68**(9-10): 864-873.
Carlstedt, J., J. Wojtasz, P. Fyhr and V. Kocherbitov (2014). "Hydration and the phase diagram of acid hydrolyzed potato starch." Carbohydrate polymers **112**: 569-577.
Chen, J., Y. Wang, J. Liu and X. Xu (2020). "Preparation, characterization, physicochemical property and potential application of porous starch: a review." International journal of biological macromolecules **148**: 1169-1181.
Chung, H.-J., K.-S. Woo and S.-T. Lim (2004). "Glass transition and enthalpy relaxation of cross-linked corn starches." Carbohydrate polymers **55**(1): 9-15.
Cornejo-Ramírez, Y. I., O. Martínez-Cruz, C. L. Del Toro-Sánchez, F. J. Wong-Corral, J. Borboa-Flores and F. J. Cinco-Moroyoqui (2018). "The structural characteristics of starches and their functional properties." CyTA - Journal of Food **16**(1): 1003-1017.
de Graaf, R. A., A. P. Karman and L. P. Janssen (2003). "Material properties and glass transition temperatures of different thermoplastic starches after extrusion processing." Starch-Stärke **55**(2): 80-86.
Drenckhan, W. and A. Saint-Jalmes (2015). "The science of foaming." Advances in Colloid and Interface Science **222**: 228-259.
Elfstrand, L., A. C. Eliasson, M. Jönsson, M. Reslow and M. Wahlgren (2006). "From starch to starch microspheres: Factors controlling the microspheres quality." Starch-Stärke **58**(8): 381-390.
Everett, D. (1972). "" IUPAC Manual of Symbols and Terminology", appendix 2, Part 1, Colloid and Surface Chemistry." Pure Appl. Chem. **31**: 578-621.
Evmenenko, G., E. Theunissen, K. Mortensen and H. Reynaers (2001). "SANS study of surfactant ordering in κ-carrageenan/cetylpyridinium chloride complexes." Polymer **42**(7): 2907-2913.
Fang, Y.-y., L.-j. Wang, D. Li, B.-z. Li, B. Bhandari, X. D. Chen and Z.-h. Mao (2008). "Preparation of crosslinked starch microspheres and their drug loading and releasing properties." Carbohydrate Polymers **74**(3): 379-384.
Fredriksson, M. and E. E. Thybring (2019). "On sorption hysteresis in wood: Separating hysteresis in cell wall water and capillary water in the full moisture range." PloS one **14**(11): e0225111.
Gao, F., D. Li, C.-h. Bi, Z.-h. Mao and B. Adhikari (2013). "Application of various drying methods to produce enzymatically hydrolyzed porous starch granules." Drying Technology **31**(13-14): 1627-1634.
Gao, F., D. Li, C.-h. Bi, Z.-h. Mao and B. Adhikari (2014). "Preparation and characterization of starch crosslinked with sodium trimetaphosphate and hydrolyzed by enzymes." Carbohydrate polymers **103**: 310-318.
Hamdi, G., G. Ponchel and D. Duchêne (1998). "An original method for studying in vitro the enzymatic degradation of cross-linked starch microspheres." Journal of controlled release **55**(2-3): 193-201.
Hirsch, J. B. and J. L. Kokini (2002). "Understanding the mechanism of cross-linking agents (POCl3, STMP, and EPI) through swelling behavior and pasting properties of cross-linked waxy maize starches." Cereal Chemistry **79**(1): 102-107.
Immel, S. and F. W. Lichtenthaler (2000). "The hydrophobic topographies of amylose and its blue iodine complex." Starch-Stärke **52**(1): 1-8.
Isleib, D. R. (1958). "Density of potato starch." American Potato Journal **35**(3): 428-429.
Kaczmarska, K., S. Żymankowska-Kumon, Ł. Byczyński, B. Grabowska, A. Bobrowski and S. Cukrowicz (2019). "Thermoanalytical studies (TG–DTG–DSC, Py–GC/MS) of sodium carboxymethyl starch with different degrees of substitution." Journal of Thermal Analysis and Calorimetry **138**(6): 4417-4425.
Kaur, L., J. Singh and N. Singh (2006). "Effect of cross-linking on some properties of potato (Solanum tuberosum L.) starches." Journal of the Science of Food and Agriculture **86**(12): 1945-1954.
Kocherbitov, V. (2021). "On the calculation of thermodynamic parameters in sorption calorimetric experiments." The Journal of Chemical Thermodynamics **152**: 106264.
Labelle, M. A., P. Ispas-Szabo and M. A. Mateescu (2020). "Structure-Functions Relationship of Modified Starches for Pharmaceutical and Biomedical Applications." Starch-Stärke **72**(7-8): 2000002.
Li, J.-X. and P. I. Lee (2006). "Effect of sample size on Case II diffusion of methanol in poly (methyl methacrylate) beads." Polymer **47**(22): 7726-7730.

Liu, J., Y. Liu, Y. Xue, Y. Ren, X. Fan, R. Wang, H. Zhang, B. Zhang and Q. Zhang (2019). "Fabrication and characterization of controllable wrinkled-surface polymer microparticles." Journal of Materials Science **54**(7): 5852-5864.

Lourdin, D., J.-L. Putaux, G. Potocki-Véronèse, C. Chevigny, A. Rolland-Sabaté and A. Buléon (2015). "Crystalline structure in starch." Starch: 61-90.

Nopens, M., L. Wadsö, C. Ortmann, M. Fröba and A. Krause (2019). "Measuring the heat of interaction between lignocellulosic materials and water." Forests **10**(8): 674.

Oliyaei, N., M. Moosavi-Nasab, A. Tamaddon and M. Fazaeli (2019). "Preparation and characterization of porous starch reinforced with halloysite nanotube by solvent exchange method." International journal of biological macromolecules **123**: 682-690.

Reddy, N. and Y. Yang (2010). "Citric acid cross-linking of starch films." Food chemistry **118**(3): 702-711.

Sandhu, K. S., A. K. Siroha, S. Punia, L. Sangwan, M. Nehra and S. S. Purewal (2021). "Effect of degree of cross linking on physicochemical, rheological and morphological properties of Sorghum starch." Carbohydrate Polymer Technologies and Applications **2**: 100073.

Singh, A. V. and L. K. Nath (2012). "Synthesis and evaluation of physicochemical properties of cross-linked sago starch." International journal of biological macromolecules **50**(1): 14-18.

Sujka, M. (2017). "Ultrasonic modification of starch–Impact on granules porosity." Ultrasonics Sonochemistry **37**: 424-429.

Sujka, M. and J. Jamroz (2007). "Starch granule porosity and its changes by means of amylolysis." International agrophysics **21**(1).

Troncoso, O. P. and F. G. Torres (2020). "Non-conventional starch nanoparticles for drug delivery applications." Medical Devices & Sensors **3**(6): e10111.

Uliniuc, A., T. Hamaide, M. Popa and S. Băcăiță (2018). "Modified Starch-Based Hydrogels Cross-Linked with Citric Acid and their use as Drug Delivery Systems for Levofloxacin." Soft Materials **11**(4): 483-493.

Wadsö, L. and N. Markova (2002). "A method to simultaneously determine sorption isotherms and sorption enthalpies with a double twin microcalorimeter." Review of scientific instruments **73**(7): 2743-2754.

Whistler, R. L. and J. R. Daniel (2000). "Starch." Kirk-othmer encyclopedia of chemical technology.

Wojtasz, J., J. Carlstedt, P. Fyhr and V. Kocherbitov (2016). "Hydration and swelling of amorphous cross-linked starch microspheres." Carbohydrate polymers **135**: 225-233.

Wulff, D. (2021). "Development of Microparticles Created from Physically Modified Starch Granules for the Uptake and Release of Drugs."

Yeh, F., E. L. Sokolov, T. Walter and B. Chu (1998). "Structure studies of poly (diallyldimethylammonium chloride-co-acrylamide) gels/sodium dodecyl sulfate complex." Langmuir **14**(16): 4350-4358.

Zhu, J., W. Sun, Z. Meng, X. Zhu, H. Gan, R. Gu, Z. Wu and G. Dou (2018). "Preparation and characterization of a new type of porous starch microspheres (PSM) and effect of physicochemical properties on water uptake rate." International journal of biological macromolecules **116**: 707-714.

Credit Author Statement

Ramūnas Digaitis: Conceptualization, Methodology, Investigation, Data Curation, Writing - Original Draft. Peter Falkman: Investigation, Visualization. Viveca Oltner: Investigation. Lars-Erik Briggner: Investigation, Methodology. Vitaly Kocherbitov: Supervision, Funding acquisition, Conceptualization, Writing - Review & Editing

Declaration of interests

☒ The authors declare that they have no known competing financial interests or personal relationships that could have appeared to influence the work reported in this paper.

☐The authors declare the following financial interests/personal relationships which may be considered as potential competing interests:

Graphical abstract